

# The Simulation of Wraparound Fins' Aerodynamic Characteristics

Minjiao Li, Laith K. Abbas, Xiaoting Rui  
 Institute of Launch Dynamics  
 Nanjing University of Science and Technology  
 Nanjing Xiaolingwei 200  
 P. R. China  
 laithabbass@yahoo.com

**Abstract:** - To study the aerodynamic characteristics of the wraparound fins, the TTCP standard wraparound fins (WAF) model was simulated using the computational fluid dynamics (CFD) method based on the shear transport (SST)  $k-\omega$  turbulent model. First, the grid independence verification was considered by using three mesh systems of different densities to calculate the model's aerodynamic coefficients. The maximum difference is within 2%. Then, the aerodynamic coefficients of the wing-wrapped vehicle model at different Mach numbers were calculated. The simulated results were compared with the experimental data, and the error could be acceptable. Finally, the WAF model's aerodynamic characteristics as a function of Mach number and angle of attack are analyzed.

**Key-Words:** - Wraparound Fins, CFD, Simulation, Aerodynamic Characteristics

## 1 Introduction

The application of wraparound fins (WAF) technology in weapon system design is becoming more extensive [1]. As often used stabilizer and control surfaces, WAF have been widely used in tactical weapons, such as antitank missile, cruise missile, etc. They could wrap around the missile body to reduce the missile's space usage before launch, fold in the early flight to reduce the drag and extend when it is needed to control the operation stability [1, 2]. These characteristics help the designers to carry on the optimal design of missiles according to the need of firing range and maneuverability. The main difference between WAF and flat fins on aerodynamics is that WAF produce rolling moment at zero angle of attack and zero installation angle which would make the body rotate around the body axis in the flight; in addition that the WAF will produce obvious yawing moment, and this moment has a strong influence over the dynamic stability of WAF vehicle.

Numerical simulation is an important means to solve aerodynamic problems at present. The computational fluid dynamics (CFD) technology can be used to analyze complex problems like three-dimensional viscous turbulent motion, vortex motion and so on. In this article, the CFD method was used to simulate the aerodynamic characteristics of the WAF model.

## 2 Modelling

### 2.1 Geometry Model

TTCP standard WAF model [3] was considered as the standard model in this present work as shown in Fig. 1, where R is the radius of the body.

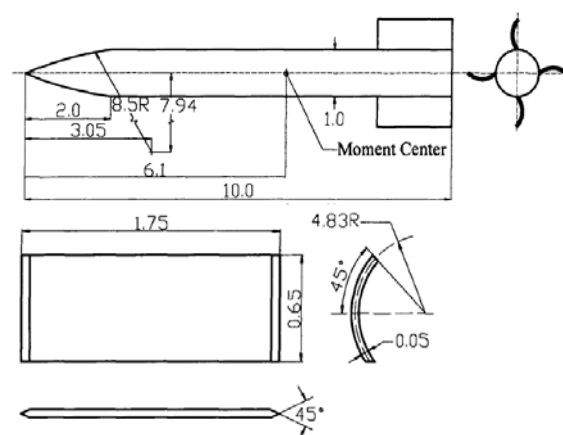


Fig.1 The model of TTCP standard WAF model

### 2.1 CFD Governing Equations

The general form of the fluid dynamics control equation can be expressed as [4]

$$\frac{\partial(\rho\phi)}{\partial t} + \text{div}(\rho\mathbf{u}\phi) = \text{div}(\Gamma \text{grad}\phi) + S \quad (1)$$

where  $\rho$  is the density,  $\mathbf{u}$  is the velocity vector,  $\phi$  is universal variable instead of the variables such as velocity, temperature,  $\Gamma$  is generalized diffusion coefficient and  $S$  is generalized source.

The terms in Eq. (1) are transient term, convection term, diffusion term and source term, respectively. By setting  $\varphi$  equal to 1,  $u_i$  and  $T$  and selecting appropriate values for diffusion coefficient  $\Gamma$  and source terms  $S$ , we obtain special forms of Eq. (1) for mass, momentum and energy conservation. The three symbols in the specific equations are shown in Table 1, where  $u_i$  is the velocity component,  $\mu$  is the dynamic viscous,  $p$  is the pressure,  $T$  is the temperature,  $k$  is the coefficient of heat conductivity,  $c$  is the specific heat,  $S_i$  is the momentum source component,  $S_T$  is the energy source term.

Table 1 The Specific Form of Each Symbol in the General Control Equation

Equations	$\varphi$	$\Gamma$	$S$
Continuity Equation	1	0	0
Momentum Equation	$u_i$	$\mu$	$-\partial p/\partial x_i + S_i$
Energy Equation	$T$	$k/c$	$S_T$

For the turbulent flow, the time average method is used to simplify the transient N-S equations. RANS equations can be written as

$$\frac{\partial \rho}{\partial t} + \frac{\partial(\rho \bar{u}_i)}{\partial x_i} = 0 \tag{2}$$

$$\frac{\partial(\rho \bar{u}_i)}{\partial t} + \frac{\partial(\rho \bar{u}_i \bar{u}_j)}{\partial x_j} = -\frac{\partial \bar{p}}{\partial x_i} + \frac{\partial}{\partial x_j} \left( -\rho \overline{u_i u_j} \right) + \frac{\partial}{\partial x_j} \left[ \mu \left( \frac{\partial \bar{u}_i}{\partial x_j} + \frac{\partial \bar{u}_j}{\partial x_i} - \frac{2}{3} \delta_{ij} \frac{\partial \bar{u}_k}{\partial x_k} \right) \right] \tag{3}$$

where  $\bar{u}_i$  is the time-average of  $u_i$ ,  $-\rho \overline{u_i u_j}$  are the Reynolds stresses

$$-\rho \overline{u_i u_j} = -\rho \begin{Bmatrix} \overline{u u} & \overline{u v} & \overline{u w} \\ \overline{v u} & \overline{v v} & \overline{v w} \\ \overline{w u} & \overline{w v} & \overline{w w} \end{Bmatrix}$$

$$= \mu_t \left( \frac{\partial \bar{u}_i}{\partial x_j} + \frac{\partial \bar{u}_j}{\partial x_i} \right) - \frac{2}{3} \delta_{ij} \left( \rho k + \mu_t \frac{\partial \bar{u}_k}{\partial x_k} \right)$$

Herein,  $u'$ ,  $v'$  and  $w'$  are the fluctuating components of  $\mathbf{u}$ ;  $\mu_t$  is the dynamic turbulent viscosity, and,  $k = \frac{1}{2} (\overline{u'^2} + \overline{v'^2} + \overline{w'^2})$  is the turbulent kinetic energy per unit mass.

Shear stress transport (SST)  $k-\omega$  turbulence model [5] combines the advantages of the standard  $k-\epsilon$  which could simulate the low Reynolds number

flow well inside the boundary layer and the standard  $k-\omega$  model which could simulate the turbulent flow outside the boundary layer. For the closure of above equations, SST model is used. Blending function is used to connect them.  $k$  and  $\omega$  transport equations can be written as

$$\frac{d(\rho k)}{dt} = \tau_{ij} \frac{\partial u_i}{\partial x_j} - \beta^* \rho \omega k + \frac{\partial}{\partial x_j} \left[ (\mu + \sigma_k \mu_t) \frac{\partial k}{\partial x_j} \right] \tag{4}$$

$$\frac{d(\rho \omega)}{dt} = \frac{\gamma \rho}{\mu_t} \tau_{ij} \frac{\partial u_i}{\partial x_j} - \beta \rho \omega^2 + \frac{\partial}{\partial x_j} \left[ (\mu + \sigma_\omega \mu_t) \frac{\partial \omega}{\partial x_j} \right] + 2\rho(1-F_1)\sigma_{\omega 2} \frac{1}{\omega} \frac{\partial k}{\partial x_j} \frac{\partial \omega}{\partial x_j} \tag{5}$$

where  $\tau_{ij} = -\overline{\rho u_i u_j}$  are the Reynolds stresses,  $\omega$  is the turbulence frequency.

Blending function  $F_1$  is given as

$$F_1 = \tanh(\arg_1^4) \tag{6}$$

where

$$\arg_1 = \min \left[ \max \left( \frac{\sqrt{k}}{0.09\omega y}, \frac{500\nu}{y^2\omega} \right), \frac{4\rho\sigma_{\omega 2}k}{CD_{k\omega}y^2} \right],$$

$$CD_{k\omega} = \max \left( 2\rho\sigma_{\omega 2} \frac{1}{\omega} \frac{\partial k}{\partial x_j} \frac{\partial \omega}{\partial x_j}, 10^{-20} \right)$$

The eddy viscosity is defined as

$$\mu_t = \frac{\rho \alpha_1 k}{\max(\alpha_1 \omega, \Omega F_2)} \tag{7}$$

where  $\Omega$  is the absolute value of the vorticity.

Blending function  $F_2$  is given as

$$F_2 = \tanh(\arg_2^2) \tag{8}$$

$$\text{where } \arg_2 = \max \left( \frac{2\sqrt{k}}{0.09\omega y}, \frac{500\mu}{\rho y^2 \omega} \right)$$

The constant  $\phi$  of the SST model is calculated from the constants shown in formula (9),

$$\phi = F_1 \phi_1 + (1-F_1) \phi_2 \tag{9}$$

where set 1 ( $\phi_1$ ) is the constant of  $k-\omega$  model, set 2 ( $\phi_2$ ) is the constant of  $k-\epsilon$  model.

The constants of set 1 ( $\phi_1$ ) are:

$$\sigma_{k1} = 0.5, \sigma_{\omega 1} = 0.5, \beta_1 = 0.075, \beta^* = 0.09, \kappa = 0.41, \gamma_1 = (\beta_1/\beta^*) - (\sigma_{\omega 1} \kappa^2 / \sqrt{\beta^*})$$

The constants of set 2 ( $\phi_2$ ) are:

$$\sigma_{k2} = 1.0, \sigma_{\omega 2} = 0.856, \beta_2 = 0.0828, \beta^* = 0.09, \kappa = 0.41, \gamma_2 = (\beta_2/\beta^*) - (\sigma_{\omega 2} \kappa^2 / \sqrt{\beta^*})$$

Other parameters are given in Ref [6].

### 2.3 The Initial and Boundary Conditions

The boundary conditions and the discrete way are important problems of solving the Euler and N-S

equations numerically, which would even cause divergence of the numerical calculation if didn't set properly. In addition, the boundary conditions have a very significant impact on the flow field accuracy. In this paper, the boundary conditions involved in the numerical simulations are: inlet boundary condition, outlet and wall boundary conditions.

In the control volume, to study the aerodynamic force regularity of the wraparound fin, the free stream condition is standard static temperature (101325 Pa) and static pressure (288 K). The boundary condition at the inlet is the far-field free stream condition, and the far-field boundary is based on Riemann invariants reflecting boundary conditions. The boundary condition of the outlet is the pressure outlet boundary condition.

For the viscous flow, the wall boundary is set by no-slip, zero pressure gradient in the normal direction and adiabatic boundary condition. The air is assumed as the ideal gas and the viscosity varies with temperature in accordance with Sutherland three coefficient formulas. Based on the density-based coupled solver, the solution method is implicit formulation and Advection Upstream Splitting Method (AUSM). AUSM is based on the finite volume method, and it's used to spatially discretize the space of the fluid field. Second Order Upwind scheme is used on convection and turbulent viscosity terms. The variable courant number technique is used during the calculation which could increase the calculating speed and guarantee the calculating stability at the same time.

## 2.1 The Grids of the Computational Field

Three mesh systems of the flow field were built-up with different densities. The grid numbers are 200 million (Mesh 1), 130 million (Mesh 2) and 340 million (Mesh 3), respectively. The mesh systems are all structured grids and the grids topologies are identical. The size of the computational field is shown in Fig. 2. To guarantee the accuracy of the computations, the boundary layer mesh is refined to ensure that the wall boundary field could be simulated precisely. The height of the first layer is 0.1 mm, and the growth factor of the height is less than 1.15. Flow field's computational grid is shown in Fig. 3. The reference area is  $A_{ref} = \pi R^2$ , where  $R$  is rocket's radius, and the reference length is  $L_{ref} = R$ , which are both the same with the references [2, 7-9].

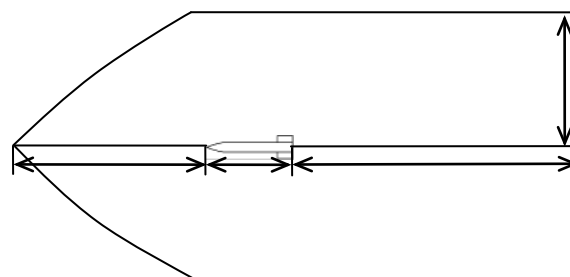


Fig.2 Computational field

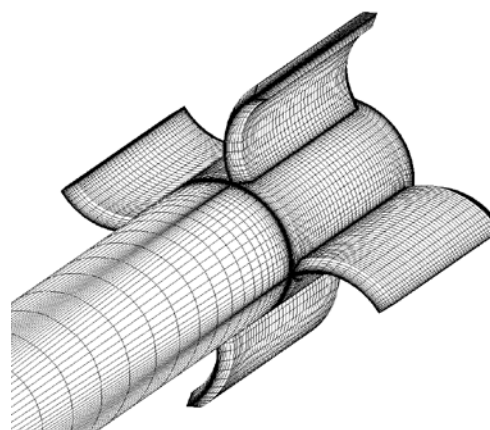


Fig.3 Discrete mesh (Mesh 2)

## 3 Presentation of the Results

### 3.1 Verification of the Grids Independence

Three mesh systems were used to simulate the WAF model under the conditions of  $0^\circ$  angle of attack and different Mach numbers by CFD method. The drag coefficients are shown in Fig. 4. From Fig. 4, it could be observed that the maximum difference of the aerodynamic results using different mesh densities is less than 2% which verifies the mesh density independence. Based on the results, the simulations of the WAF model use Mesh 2.

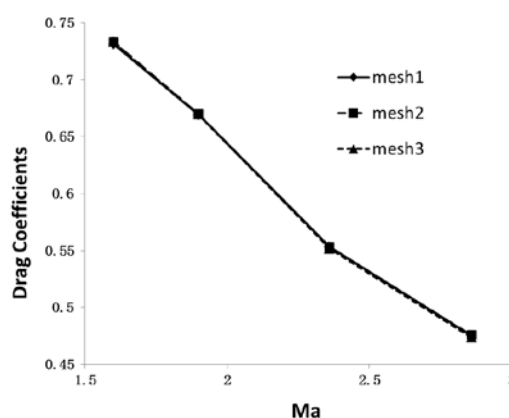


Fig.4 Drag coefficients of the model at  $0^\circ$  angle of attack with three mesh systems

### 3.2 Verification of the CFD Method

Figures 5 and 6 show the drag coefficients  $C_{Df}$  of the fins and the rolling moment coefficients  $C_{mx}$  of the whole model calculated in this paper and the results from reference [3, 7-9]. The maximum error of  $C_{Df}$  is less than 10% compared with the reference [3].  $C_{mx}$  agree well with the results of the reference and the experiments [7-9], which reflects the accuracy of the CFD method in this paper.

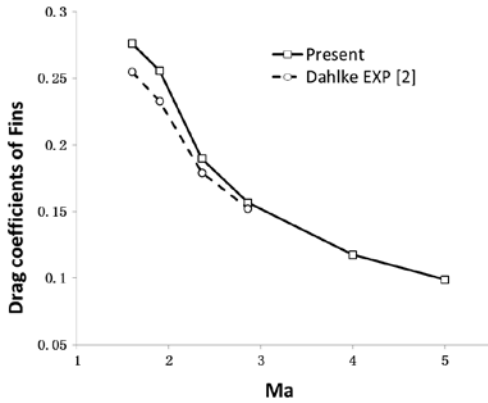


Fig.5 Drag coefficients of the fin at 0° angle of attack

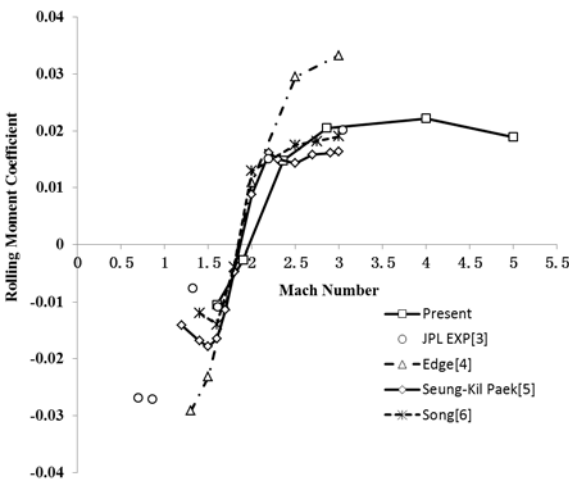


Fig.6 The model's rolling moment coefficient at 0° angle of attack

### 3.3 The Aerodynamic Characteristics of the WAF Model

The aerodynamic characteristics are calculated under the conditions of 0° angle of attack and different Mach numbers (3 and 5). The Mach number contour maps are shown in Figs. 7-8. With the increase of incoming flow's Mach number, the strength of the shockwave at the nose becomes strong and the shock wave angle becomes smaller. Figure 9 is the pressure contour of the WAF model of 5 Ma from which it is clear that the pressure on

the concave surface is higher than the pressure on the convex surface producing the rolling moment at 0° angle of attack.

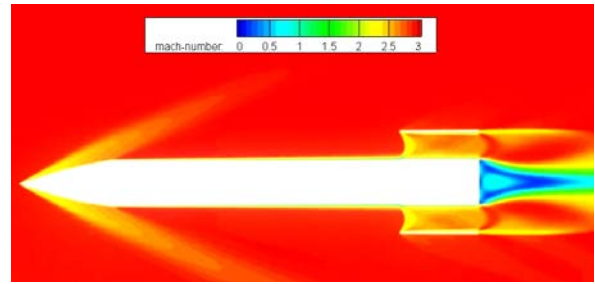


Fig.7 The Mach number contour of the WAF model at 0° angle of attack and Ma=3

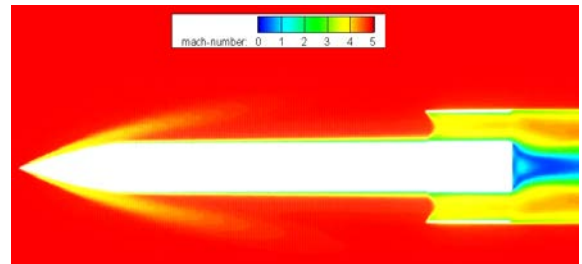


Fig.8 The Mach number contour of the WAF model at 0° angle of attack and Ma=5

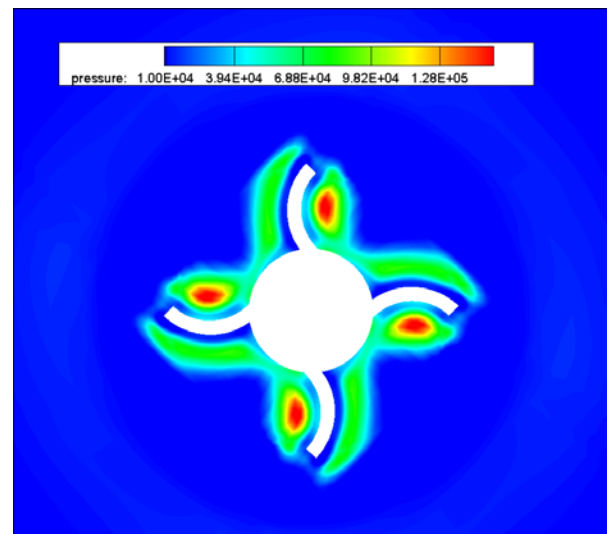


Fig.9 The pressure contour of the model under the condition at 0° angle of attack and Ma = 5

The drag coefficient  $C_D$ , lift coefficient  $C_L$ , lateral force coefficient  $C_z$  and the rolling moment coefficient  $C_{mx}$  of the WAF model were obtained, and the results are shown in Figs. 10-13. The characteristics law of the WAF model under hypersonic speed could be observed by analyzing Figs. 10-13. Under the given Mach numbers, the relationship of  $C_D$  with the angle of attack appears to be parabolic curves. At the same angle of attack,

higher Mach number leads to smaller  $C_D$  and  $C_L$ . With the increasing of Mach number, the relation of  $C_L$  and the angle of attack tend towards to linearization.

According to the results in Fig. 12, with the increasing of Mach number,  $C_z$  becomes larger when the angle of attack is smaller than  $10^\circ$ , but this trend is opposite when the angle of attack is larger than  $10^\circ$ . This shows that the WAF lead to larger yawing moment at the hypersonic speed and large angle of attack which calls for high requirement of the control and stability.

Figures 6 and 13 indicate that at a given Mach number, the rolling moment coefficient  $C_{mx}$  has nonlinear growth with the increasing of the angle of attack. From the results, the WAF at hypersonic speed don't have higher requirement of control of the flying vehicle's rolling channel.

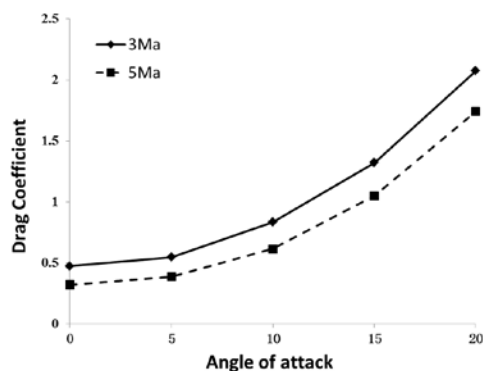


Fig.10 The Lift coefficients of the WAF model

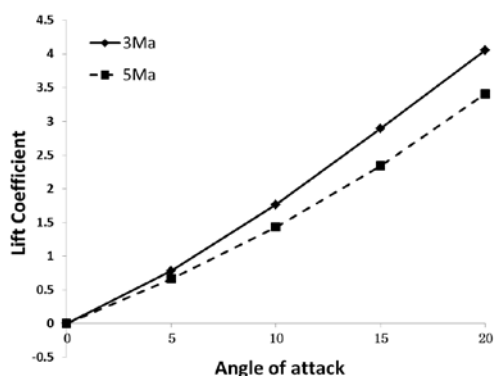


Fig.11 The Drag coefficients of the WAF model

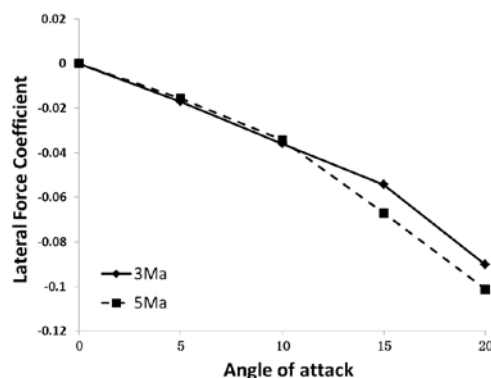


Fig.12 The lateral force coefficients of the WAF model

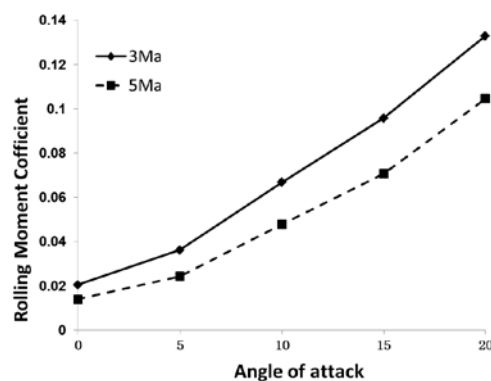


Fig.13 The rolling moment coefficients of the WAF model

### 4 Conclusion

The aerodynamic characteristics of the TTCP standard WAF model from 1.6Ma to 5Ma and at different angles of attack are obtained by CFD method. Part of the results was verified by comparing to the published literatures and the experiment results. For the same angle of attack, the drag, lift and rolling moment coefficients are smaller at higher Mach number. The WAF at hypersonic speed don't lead to higher requirement of control for the flying vehicle's rolling channel. However, the WAF lead to larger lateral force and yawing moment at hypersonic speed and large angle of attack, which calls for high requirement of the control and stability.

### Acknowledgement

The research was supported by the Research Fund for the Doctoral Program of Higher Education of China (20113219110025, 20133219110037), the Natural Science Foundation of China Government (11472135, 61304137), and the Program for New Century Excellent Talents in University (NCET-10-0075).

*References:*

- [1] Wu, J. S., Ju, X. M., Xu, W. X., "Self- Rolling Characteristics of Wrap Around Fin-Body Combinations," *Journal of Beijing Institute of Technology*, 13(2(1)), 1993, pp. 180-186.
- [2] Song, X. M., Xia, G., "Numerical Simulation of Flow Field for Wraparound Fins Projectile at Zero Angle of Attack," *Tactical Missile Technology*, 6, 2002, pp. 21-24.
- [3] Dahlke, C. W., "The effect of Wrap-Around fins on aerodynamic stability and rolling moment variations," AD-76758, 1973.
- [4] Zhang. S. S., Fluid dynamics and application. Huazhong University of Science and Technology Press Wuhan, 2011, pp. 5-10
- [5] MENTER F R., "Zonal two equation k- $\omega$  turbulence models for aerodynamic flows," AIAA-93-2906, 1993.
- [6] Menter. F. R., "Two-equation eddy-viscosity models for engineering applications," *AIAA Journal*, 32, 1994, pp. 1598-1605.
- [7] Dahlke, C. W., "The Aerodynamic Characteristics of Wrap-Around Fins at Mach Number of 0.3 to 3.0," U. S. Army Missile Command, TR RD-77-4, Redstone Arsenal, AL, Oct. 1976.
- [8] Edge, H. L., "Computation of the Roll Moment for a Projectile with Wrap-Around Fins," *Journal of Spacecraft and Rockets*, 31(14), 1994, pp. 615-620.
- [9] Paek, S. K., Park, T. S., "Computation of Roll Moment for Projectile with WAF Using Euler Equation," *Journal of Spacecraft and Rockets*, 36(1), 1999, pp. 53-58.